Evolution of Dual-Pol Radar Signatures of QLCS Tornado Development

Olivia F. McCauley[1], Charles M. Kuster[2,3,4], Vivek N. Mahale[5], and Terry J. Schuur[2,3,4]

[1]National Weather Center Research Experiences for Undergraduates Program, Norman, Oklahoma
[2]Cooperative Institute for Mesoscale Meteorological Studies, Norman, Oklahoma
[3] NOAA/OAR/National Severe Storms Laboratory, Norman, Oklahoma
[4]University of Oklahoma, Norman, Oklahoma
[5]NOAA/National Weather Service, Norman, Oklahoma

ABSTRACT

The purpose of this study is to identify and analyze potential radar base and dual-polarization precursor signatures for quasi-linear convective system (QLCS) tornadoes. QLCS tornadoes present many forecasting challenges based on their rapid development, transience, and dynamic environment. QLCS tornadoes can form in between radar scans so it is imperative to forecasters to locate potential key radar signatures to issue tornado warnings in advance of tornadogenesis. Having the ability to detect early radar signatures of QLCS tornado development can potentially increase tornado warning lead time to the public and help those in danger better prepare for the risks tornadoes pose. Radar analysis was conducted using the Warning Decision Support System (WDSS). Base products used were spectrum width, reflectivity, and velocity; dual-pol products used were correlation coefficient, differential reflectivity (Z_{DR}), and specific differential phase (K_{DP}). There were a total of 18 tornadic mesovortices and 5 non-tornadic mesovortices studied. The analysis showed that the most beneficial radar precursor signatures may be Z_{DR} columns, enhanced areas of K_{DP} around developing mesovortices, updraft/downdraft convergence zones along the leading edges of QLCSs, as well as concentrated areas of enhanced spectrum width at the low levels.

1. INTRODUCTION

Quasi-linear convective systems (QLCSs) encompass squall lines as well as bow echoes that develop out of a series of short lived but highly interactive cells (Trapp et al. 2005). To be classified as a QLCS, these cells must have reflectivity of 40 dBZ or higher distributed continuously over a horizontal distance of at least 100 km (Trapp et al. 2005). The motion and accompanying dynamics of a QLCS is highly predicated on the production of a surface-based cold pool by the interacting cells within it (Weisman and Trapp 2003). However, one caveat to this system is that the motion of the QLCS and that of its individual cells can be different from one another (Bluestein and Jain 1985). The most pertinent feature of the cold pool is that it produces a temperature gradient on a constant pressure surface, also known as a baroclinic zone. Horizontal shear generated along this baroclinic zone can be tilted and stretched by an updraft to from vertically oriented circulations called mesovortices (Weisman and Trapp 2003). The birth of mesovortices most frequently occurs in a low-level cyclonic-convergent area located along the leading edge at the apex of a bow echo. As vortices mature, they undergo strengthening and deepening while moving northward in step with the bow apex. Weakening and subsequent dissipation features vortex broadening with a propensity for rearward motion relative to the line as new convective cells and low-level mesovortices form along the front of the bow apex (Funk et al. 1999). The study also concluded that many different circulations could coexist at the same time at differing stages of QLCS evolution. Some of these circulations can attain mesocyclone criteria, which is commonly associated with tornadogenesis in supercells. In addition, tornadoes tend to occur in tandem with intensification and deepening of low-level vortices (Funk et al. 1999).

Within QLCSs, small-scale mesovortices have a tendency to organize at low-levels (i.e., up to 3 km above ground level) typically north of the apex of a bow echo but also occasionally south of the apex (e.g., Przybylinski 1995; Przybylinski et al. 2000; Atkins et al. 2004). Mesovortices differ from mesocyclones in that they build upward and are not associated with rotating updrafts that are long-lived at the midlevels, as is typical in supercells (Mahale et al. 2012). Mahale et al. (2012) also noted that these mesovortices can have strengths similar to mesocyclones. Mesovortices in QLCSs tend to develop in environments that feature stout, low- to midlevel (from 2.5 to 5 km) vertical wind shear greater than 20 m s^{-1} and can enhance straight-line wind damage potential where they are located along the squall line (Weisman and Trapp 2003). This enhancement of straight-line wind damage along the right side of mesovortices comes from the mesovortex having lateral movement alongside the squall line (Wakimoto et al. 2006; Mahale et al. 2012).

In terms of the quantification of QLCS tornadoes, Trapp et al. (2005) conducted a study including 3,828 tornadoes and uncovered the fact that 18% of them occurred within QLCS events. Most of the tornadoes were F1 tornadoes (the study excluded F0 tornadoes) while some met or exceeded F2 intensity, however F3 and F4 tornadoes were noted to be rare. Smith et al. (2010) established that 12.1% of all tornadoes between 2003 and 2009 were associated with QLCSs. The study also made a clear separation between tornadoes associated with embedded supercells within a line and those associated with QLCSs. Trapp et al. (1999) also showcased that tornadogenesis from mesovortices often occurs at a much more rapid rate than those from supercells, with an average lead time of about five minutes. Work by Atkins et al. (2004) also suggests that a thorough analysis of radar data might allow one to differentiate between mesovortices that are tornadic and nontornadic because tornadic mesovortices tend to be stronger, longer-lived, and deeper than other nontornadic mesovortices within the same or different events. Therefore, it may be important to identify and differentiate between well-established mesovortices and ones that are weaker and more transient.

The purpose of this study is to examine dual-polarization (dual-pol) Weather Surveillance Radar-1988 Doppler (WSR-88D) radar data for multiple QLCS events to identify potential tornadogenesis precursor signatures that may be useful during real-time tornado-warning

[1] *Olivia McCauley, Mount Holyoke College, mccau22o@mtholyoke.edu*

operations. QLCS tornadoes provide a unique forecast challenge due to their dynamic nature, rapid evolution, and detection limitations. We therefore seek to aid forecasters in increasing QLCS tornado lead time by examining many different radar signatures in the context of warning decision making. Determining differences in these signatures between tornadic and nontornadic mesovortices may also prove key to increasing probability of detection while also lowering the false alarm rate.

2. RADAR DATA AND SIGNATURES

Radar data from four different radars—KTLX in Oklahoma City, OK, KOUN in Norman, OK, KFDR in Fredrick, OK, and KENX in Albany, NY—were displayed and analyzed using the Warning Decision Support System-Integrated Information (WDSS-II) software program (Lakshmanan et al. 2007). Three of these radars (KENX, KFDR, and KTLX) collected 360° volume scans using volume coverage pattern (VCP) 212 (Table 1). In each case, radar operators used a special scanning strategy called Supplemental Adaptive Intravolume Low-Level Scans (SAILS; Crum et al. 2013) or Multiple Elevation Option for SAILS (MESO-SAILS; Chrisman 2014), which interrupts the volume scan to add in additional low-level (i.e., 0.5°) scans. These strategies produced update times of about 1.5 to 2.5 min for the lowest elevation angle and about 5 to 6.5 min for the full volume scan. Since KOUN is a research WSR-88D, radar operators are able to perform 90° sector scans and use specialized VCPs that result in volumetric updates times of about 1.5 min (Table 1).

To examine various signatures associated with QLCS mesovortices, we utilized several single-pol and dual-pol variables. Reflectivity, which displays echo intensity in decibels (dBZ), was primarily used to evaluate storm structure and precipitation detection. Base velocity, was used to detect mesovortices, rear inflow jets (RIJ) which are descending jets of strong winds on the backside of a QLCS, and updraft/downdraft convergence zones (Fig. 1c; Fig. 2). Spectrum width (SPW) measures the distribution or dispersion of velocities and was used to identify concentrated local shear zones associated with each mesovortex (Fig. 1b). Differential Reflectivity (Z_{DR}), a ratio of both the horizontal and vertical polarization of a hydrometer, was employed to determine the location of Z_{DR} columns and Z_{DR} arcs (Fig. 3a, b; e.g., Kumjian et al. 2008). Z_{DR} columns, usually collocated with updrafts, are columns of supercooled liquid rain drops lofted above the melting layer (environmental 0 degrees Celsius level) by these updrafts (Snyder et al. 2015). Z_{DR} columns can therefore be indicative of updraft location and intensity and potentially provide insight into mechanisms such as hail growth or stretching of vertical vorticity (e.g., Picca et al. 2010; Snyder et al. 2015). Specific Differential Phase (K_{DP}), a measure of differential phase shift over a unit distance, is a good indicator of liquid water content within a radar volume and is therefore useful for identifying areas of heavy rainfall. For example, in this study high K_{DP} located near a mesovortex could indicate a rainy downdraft that may increase baroclinic vorticity prior to tornadogenesis (Fig. 3c; e.g., Trapp and Weisman 2003). Lastly, Correlation Coefficient (ρ_{hv}) shows the consistency in the shapes and sizes of radar targets and was used to help identify tornado debris signatures. All information about reported tornadoes up to April 2019 was gathered from the National Centers for Environmental Information's Storm Events Database (available at https://www.ncdc.noaa.gov/stormevents/ftp.jsp) and from the Storm Prediction Center's preliminary storm reports (available at https://www.spc.noaa.gov/climo/online/) for any event after April 2019.

3. RADAR ANALYSIS AND RESULTS

3.1 *25 February 2017 (Western Massachusetts)*

On the evening of 25 February 2017 a squall line began to move through western Massachusetts. From 2335 to 2348 UTC the north bowing segment of the squall line entered southern Berkshire County. Behind this bowing segment was a strong RIJ. Accompanying this bowing section was a broad arc of Z_{DR} that indicated large raindrops within the line. At 2349 UTC, broad rotation was evident along an updraft/downdraft convergence zone near the apex of the bowing segment. By 2351 UTC, this rotation intensified and a mesovortex formed in south central Berkshire County but did not produce a tornado. Within the following minutes two areas of enhanced K_{DP} formed to the north and south of this maturing mesovortex. Both K_{DP}

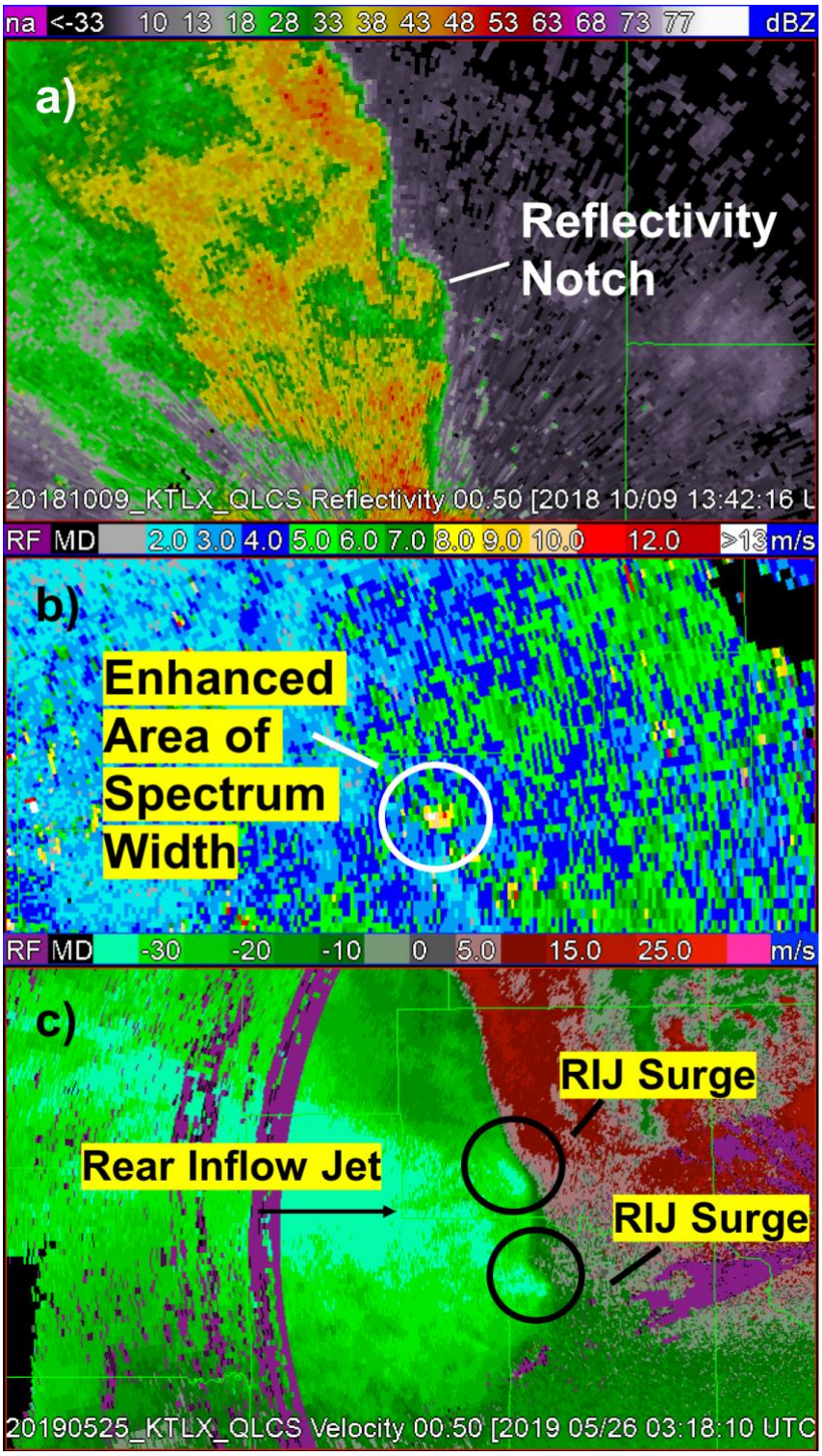

Fig. 1. Example of a) reflectivity notch on 9 October 2018, b) concentrated area of enhanced spectrum width on 18 May 2019, and c) rear inflow jet and RIJ surges on 26 May 2019.

Table 1. Radar information for all analyzed cases.

Date	Radar	VCP/Elevation Angles	Approx 0.5 Degree Update Time	Approx Volume Update Time
25-26 Feb. 2017	KENX	212	2 min 10 sec	6 min 10 sec
3 May 2018	KTLX/KOUN	KTLX: 212 KOUN: 0.5, 0.9, 1.4, 2.4, 3.5, 4.6, 5.7, 7.1, 9.1, 11.4	KTLX: 1 min 30 sec KOUN: 1 min 30 sec	KTLX: 6 min 30 sec KOUN: 1 min 30 sec
9 Oct. 2018	KTLX	212	2 min 30 sec	5 min 0 sec
18 May 2019	KFDR	212	1 min 50 sec	6 min 15 sec
21 May 2019	KTLX	212	1 min 30 sec – 2 min 0 sec	6 min 0 sec – 6 min 15 sec
26 May 2019	KTLX	212	1 min 30 sec – 2 min 30 sec	5 min 10 sec – 6 min 30 sec

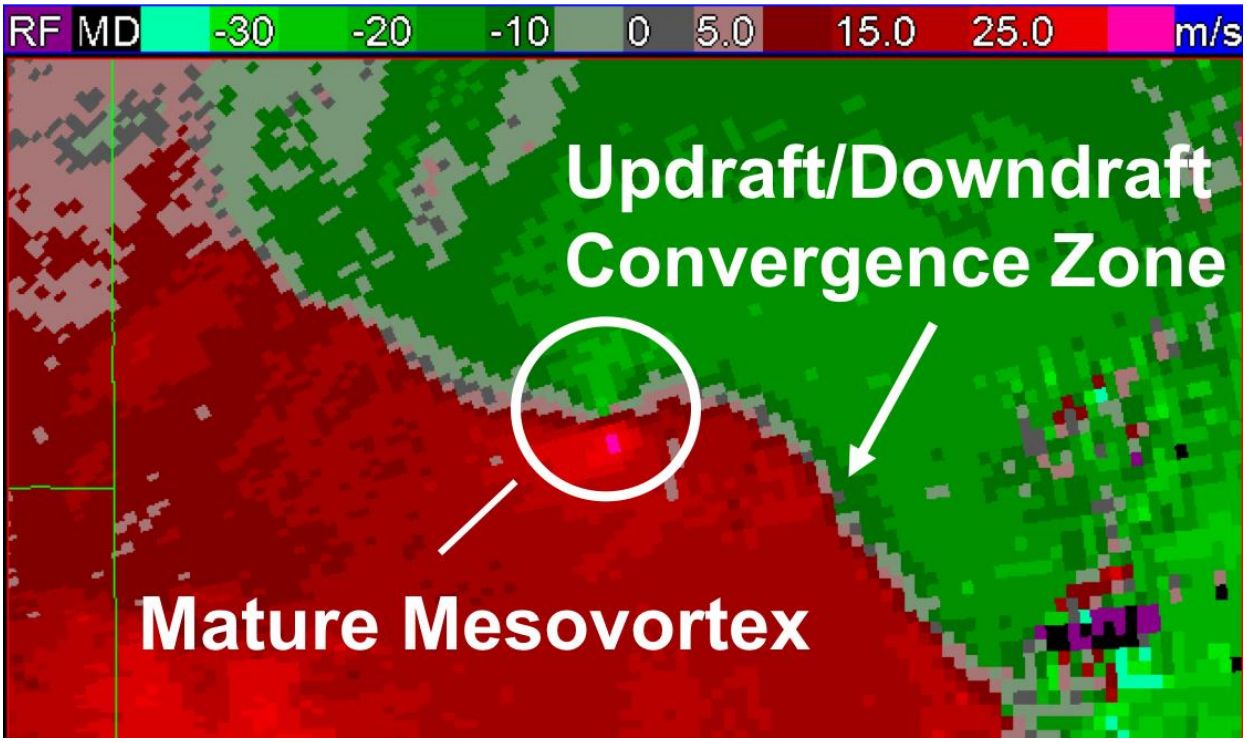

Fig. 2. Example of a mature mesovortex and updraft/downdraft convergence zone on 21 May 2019.

and Z_{DR} decreased as the bowing segment and mesovortex along the apex moved eastward.

At 0010 UTC the bow began to enter portions of western Hampden and Hampshire Counties. Rotation associated with the mesovortex increased, however, there was no prior concentrated area of enhanced spectrum width. Velocity then indicated further strengthening of the mesovortex to its maximum strength between 0016 UTC and 0018 UTC. At 0018 UTC gate-to-gate shear associated with the mesovortex reached 61 m s^{-1}, in part due to the rapid velocity of the RIJ which surged the bow to the northeast, and a tornado developed in Goshen, MA. This tornado dissipated three min later at 0021 UTC as the mesovortex briefly weakened. The mesovortex then restrengthened at 0022 UTC along the updraft/downdraft convergence zone and produced another tornado that began at 0023 UTC in South Ashfield, MA, and ended at 0027 UTC. Throughout this four minute period, there was a lowering of squall line cloud tops on reflectivity,

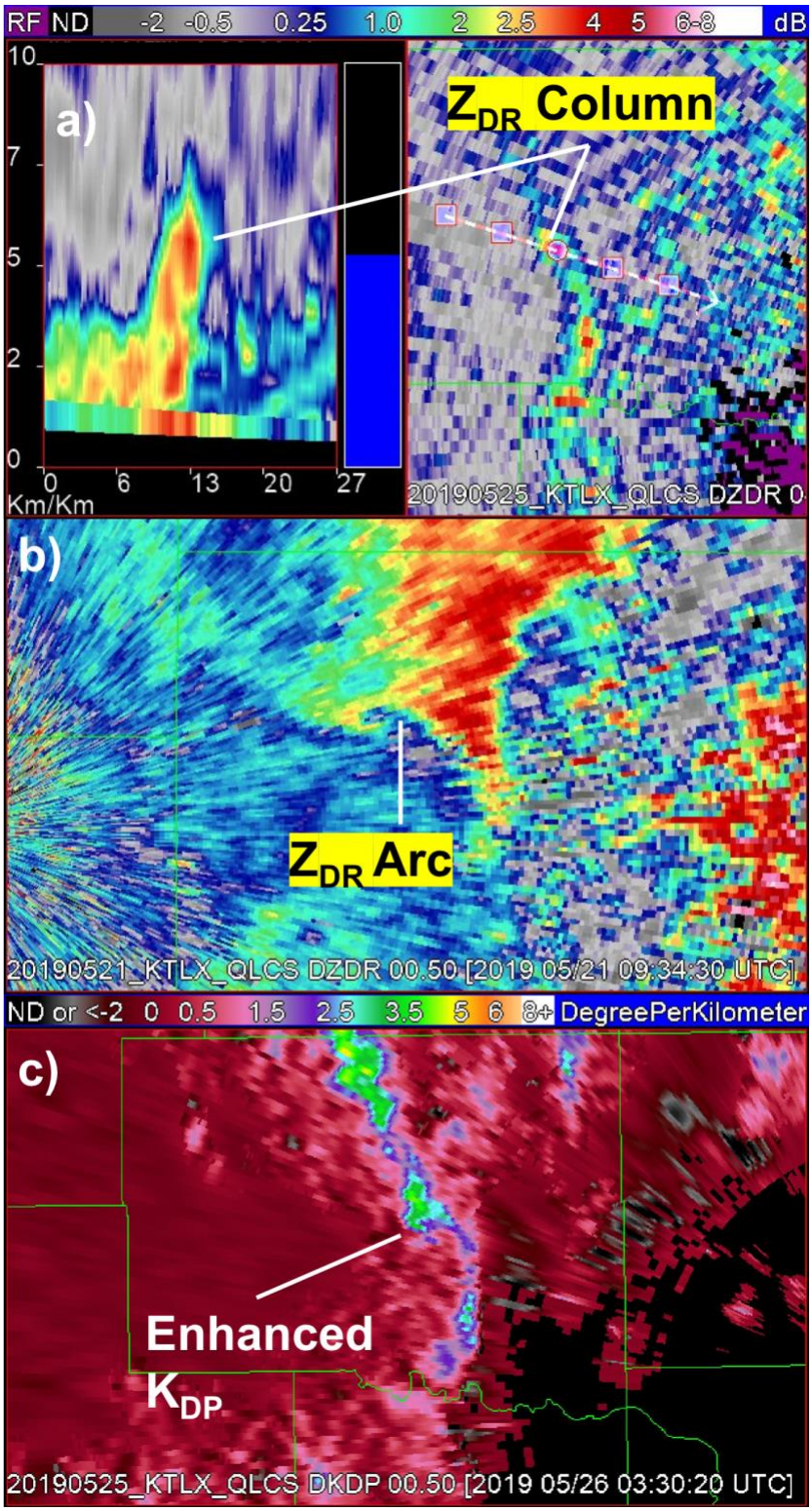

Fig. 3. Example of a) a Z_{DR} column on a quasi-vertical profile (left panel) and planned position indicator (PPI; right panel) on 26 May 2019, b) a Z_{DR} arc on 21 May 2019, and c) an area of enhanced K_{DP} just north and north west of a mesovortex that occurred on 26 May 2019. Color bar for Z_{DR} in a) and b) is located at the top of the figure.

which coincided with decreased K_{DP} and Z_{DR} values along the bow apex (0.5° elevation). By 0027 UTC, the bow weakened as the RIJ dissipated.

3.2 *3 May 2018 (Central Oklahoma)*

During the late afternoon of 2 May 2018, discrete cells formed along a dry line in the western Oklahoma and Texas panhandles. Through the late evening the discrete cells grew upscale into a line that moved through southwest and central Oklahoma. A total of three tornadoes were produced by this squall line in central Oklahoma.

A slight convergence zone existed on the border of McClain and Cleveland Counties at 0130 UTC with generally low K_{DP} and Z_{DR} values within the same area. There was also a Z_{DR} column at the southern end of a bowing section of the squall line that had advanced eastward at 0132 UTC into northwestern Cleveland County. A Z_{DR} arc was observed at 0.5 degrees directly beneath the Z_{DR} column. At 0134, the RIJ surged out directly to the west of where the notch was located along the bowing structure and a Z_{DR} column was observed to the east of the notch. The Z_{DR} column was apparent right before a tornado was produced by 0142 UTC two miles to the north northeast of Norman as the RIJ intensified and enhanced the rotation associated with the mesovortex.

A mesovortex began to develop in north central McClain County at 0138 UTC when a slight reflectivity notch (e.g., Fig. 1a) formed along the leading edge of a squall line. There was a weak area of enhanced spectrum width with this mesovortex as well as an area of high K_{DP} just southwest of the mesovortex. A well-defined Z_{DR} column was noted at 0144 UTC, or about 4 min prior to tornadogenesis. Right before tornadogenesis occurred at 0148 UTC near Purcell, an area of high K_{DP} formed directly northwest of the mesovortex.

Another weaker mesovortex developed in southern McClain County, south of Asher, as the northern mesovortex produced a tornado. This mesovortex also existed on a reflectivity notch along the southern end of the squall line and was associated with an RIJ surge (e.g., Fig. 1c). Even though there was a concentrated area of enhanced spectrum width and a Z_{DR} column at 0153 UTC, a tornado never formed from this mesovortex and it dissipated shortly afterwards.

To the east, a mesovortex developed at 0208 UTC. A concentrated area of enhanced spectrum width existed along a clear updraft/downdraft convergence zone in the center of Pottawatomie County. An area of high K_{DP} developed south of the mesovortex as a slight reflectivity bulge appeared through 0211 UTC. This area of K_{DP} increased as inbound winds met up with outbound winds, increasing mesovortex rotation dramatically. A tornado was produced from this mesovortex near Macomb between 0218 UTC and 0219 UTC. The mesovortex and SPW reached max strength when the tornado was in progress, weakening when the tornado dissipated south of Brooksville.

3.3 *9 October 2018 (Central Oklahoma)*

During the morning of 9 October 2018, a narrow northwest to southeast oriented, fast-moving, low-topped squall line moved through central Oklahoma, producing several EF0 and EF1 tornadoes along its path. K_{DP} and Z_{DR} were quite low along the squall line and no Z_{DR} columns or arcs were observed. This lack of noteworthy dual-pol signatures may be due to lower data quality due to widespread ground clutter where the storms occurred. Despite the lack of clear dual-pol signatures, we frequently observed concentrated areas of enhanced SPW prior to tornadogenesis. The first of seven tornadoes was produced by a mesovortex that formed along a slight updraft/downdraft convergence zone at one of several reflectivity notches along the length of the squall line. About five min before this tornado began, a concentrated area of enhanced SPW was observed. The gate-to-gate couplet of this tornado was relatively weak and the tornado only lasted one minute. Shortly thereafter, another mesovortex rapidly developed and intensified just to the south and east along the convergence zone. At first, this mesovortex was quite weak and no concentrated area of enhanced SPW was noted before tornadogenesis. As the mesovortex intensified, a tornado developed at 1328 UTC two miles north northwest of Tinker Air Force Base and lasted for 18 min. This long-lived QLCS tornado was associated with a long-lived mesovortex and a tornado debris signature (TDS).

While this long-lived tornado was ongoing, another weak tornado occurred about 5 miles south-southeast of Edmond, OK at 1333 UTC. Similarly to the first tornado near Oklahoma City, a concentrated area of enhanced SPW occurred

about four min prior to tornadogenesis. Yet another mesovortex formed to the south of the long-lived mesovortex that produced the Tinker AFB tornado. This mesovortex also rapidly developed along a leading edge reflectivity notch. Once again, a concentrated area of enhanced SPW was observed about two min prior to a tornado developing near Choctaw, OK at 1342 UTC. A TDS was also detected at 1344 UTC.

Farther south along the updraft/downdraft convergence zone in Cleveland County, three different mesovortices formed and produced tornadoes with the third not producing a tornado until it reached Prague, OK in Lincoln County. The first of the two deeper mesovortices was located along the leading edge of the squall line within a reflectivity notch. A concentrated area of enhanced SPW was observed six min prior to this mesovortex producing a tornado near Little Axe, OK at 1330 UTC. At nearly the same time, a concentrated area of enhanced SPW was observed at 1329 UTC with the second mesovortex that produced a tornado two min later near Stanley Draper Lake. As the squall line tracked east into Pottawatomie County, it produced one more brief tornado in Prague, OK. No concentrated areas of enhanced SPW were observed prior to this brief tornado.

3.4 *18 May 2019 (Southwestern Oklahoma)*

Through the morning of 18 May 2019, a squall line moved across southwestern Oklahoma and produced one EF2 tornado over Geronimo. At 1226 UTC, a Z_{DR} column was located in north central Cotton County. At this time, there were no concentrated areas of enhanced SPW, but two did develop by 1231 UTC and were associated with two mesovortices. When the northernmost (Geronimo mesovortex) of the two mesovortices began to strengthen at 1233 UTC, the southernmost one dissipated. The concentrated area of enhanced SPW associated with the Geronimo mesovortex also became much more dominant than the one associated with the southern mesovortex. A tall updraft, marked by a Z_{DR} column, existed over the northernmost mesovortex right before the Geronimo mesovortex produced a tornado sometime between 1235 and 1239 UTC. The first sign of a TDS occurred at 1239 UTC.

3.5 *21 May 2019 (Central Oklahoma)*

On 21 May 2019, a QLCS tracked trough Oklahoma overnight and produced five different tornadoes within McClain, Cleveland, and Pottawatomie Counties. At 0833 UTC, a line of enhanced K_{DP} developed in eastern Grady County. The northernmost section of this line in central McClain County featured the highest K_{DP} values. Proximal to the highest K_{DP} values was a very tall and vigorous updraft, marked by a Z_{DR} column that was associated with what would later become a tornadic mesovortex. By 0841 UTC there was a noticeable expansion in K_{DP} and Z_{DR} values in north central McClain County to the west of a quickly developing mesovortex. These areas of enhancement were not as intense as those associated with mesovortices later in the data set and the rotational couplet was also much more subtle in comparison to the rotational couplets of subsequent mesovortices. At 0843 UTC, two min prior to tornadogenesis, there was a small concentrated area of enhanced SPW to the southwest of Goldsby, OK as well as a further enhancement of K_{DP}. Just before tornadogenesis, the Z_{DR} column intensified. A tornado formed at 0845 UTC alongside a more significant increase of K_{DP} into a wedge to the north of the mesovortex.

After the dissipation of the Goldsby-Noble tornado, two different Z_{DR} columns were present on radar at 0851 UTC. The southernmost Z_{DR} column was associated with the Goldsby-Noble tornado, the other to the north was associated with another developing tornadic mesovortex (Norman mesovortex). A significant area of enhanced K_{DP} continued to the north and west through 0855 UTC, while another area of enhanced K_{DP} developed to the south and east of two different bulges on reflectivity associated with the Goldsby-Noble mesovortex and the Norman mesovortex. These two bulges looked to be the resultant of RIJ surges as the bowing region of the squall line accelerated off to the northeast. By 0857 UTC a tornado was produced by the Norman mesovortex. The velocity couplet intensified through 0905 UTC and a tornado debris signature was present by this time.

Several min later, at 0920 UTC, the northern Cleveland County mesovortex developed just to the northeast of KTLX and was accompanied by a slightly defined Z_{DR} arc. An arc of enhanced SPW with a concentrated area of enhanced SPW at the tip of the arc was present two min prior to tornadogenesis that occurred at 0922 UTC. This concentrated area of SPW reached its maximum magnitude at 0927 UTC and

a Z_{DR} arc and area of enhanced K_{DP} also continued after tornadogenesis.

The updraft/downdraft convergence zone became a feature to hone in on due to the fact that a very clear inflow notch had materialized at 0929 UTC along the convergence zone where the Z_{DR} arc existed, all under the influence of the RIJ surge. At 0930 UTC, rapid mesovortex development occurred and a Z_{DR} column was associated with this mesovortex. Similarly to the previous mesovortex, a concentrated area of enhanced SPW was located at the tip of an arc of enhanced SPW about two min prior to tornadogenesis, which occurred at 0932 UTC. To the east of the mesovortex, the Z_{DR} arc became more organized along with a defined curl of liquid droplets as indicated by enhanced K_{DP} around the mesovortex. After moving over Dale, the mesovortex occluded back to the west as and another similar process ensued for a succeeding mesovortex over eastern Pottawatomie County.

At 0942 UTC another inflow notch formed at the bow apex and a Z_{DR} column was detected over northeastern Pottawatomie County. Z_{DR} and K_{DP} organized and intensified at the bow apex by 0945 UTC while the mesovortex traveled closer into the inflow notch. A hook echo structure became apparent a minute later at this location. Immediately before tornadogenesis, a Z_{DR} column was colocated with the mesovortex and the concentrated area of enhanced SPW intensified within the inflow notch. The final tornado formed at 0950 UTC three miles to the east northeast of Aydelotte with a clear Z_{DR} arc to the east, similar to the Dale mesovortex.

3.6 *25 May 2019 (Central Oklahoma)*

During the late evening hours of 25 May 2019, a squall line moved through central Oklahoma and produced several tornadoes including an EF3 that impacted El Reno, OK. At 0312 UTC, two subtle reflectivity notches became apparent, and both were associated with mesovortices and RIJ surges (Fig. 1c). The northern mesovortex was associated with the El Reno tornado, while the southern mesovortex was nontornadic. A Z_{DR} column existed with the northern mesovortex while the southern mesovortex only had a weak and diffuse Z_{DR} column. A concentrated area of enhanced SPW was already apparent with the northern mesovortex as 0313 UTC—about 13 min prior to tornadogenesis—but such a signature was not observed with the southern nontornadic mesovortex. These two reflectivity notches gained more definition over subsequent volume scans with high low-level (0.5° tilt) Z_{DR} and K_{DP} values proximal to the northern mesovortex much more than the southern mesovortex. The northern mesovortex also existed on a much more prevalent updraft/downdraft convergence zone than the southern mesovortex, which may have enhanced rotation, especially since it existed on the apex of a bowing structure within the squall line. The northern mesovortex continued to intensify as the RIJ surged out ahead of the convergence zone, and the El Reno tornado developed at about 0326 UTC. At this time, a subtle ring of K_{DP} began to surround the mesovortex at the 0.5° elevation angle and a Z_{DR} column was still present. At 0327 UTC, the K_{DP} ring intensified, curling around the mesovortex reaching peak definition at 0330 UTC. A significant TDS was also observed with this tornado.

After the El Reno tornado dissipated, the squall line continued into Oklahoma County and another mesovortex developed. Enhanced low-level (0.5° elevation angle) Z_{DR} and K_{DP} persisted just west and west-northwest of the developing mesovortex and a concentrated area of enhanced SPW was noted at 0345 UTC. The RIJ continued to surge, although not as intense as earlier and a Z_{DR} column was observed at the 0351 UTC, or about two min prior to tornadogenesis at 0353 UTC near Del City, OK. No TDS was observed with this tornado.

4. CONCLUSION

A total of 23 different mesovortices were studied across 6 QLCS events. Of those 23 mesovortices, 18 were tornadic and 5 were non-tornadic. The presence of a Z_{DR} column correlated to tornadic mesovortices with a 75% occurrence rate verses 50% with mesovortices that did not produce tornadoes (Table 2). If data quality issues were removed, then high K_{DP} areas occurred in the proximity of 83% of tornadic mesovortices and 50% of non-tornadic mesovortices. A concentrated area of enhanced spectrum width occurred more frequently (78%) among tornadic mesovortices prior to tornadogenesis compared to nontornadic mesovortices (60%). All of the mesovortices that produced tornadoes were long lived and established while 80% of non-tornadic mesovortices were transient and weaker. In instances were two mesovortices existed along a

bowing segment, the northern mesovortex near the bow apex dominated and became tornadic. Since all mesovortices were associated with RIJ surges, future work could examine and quantify the magnitude of the RIJ surge associated with each mesovortex. The majority (83%) of tornado producing mesovortices formed on updraft/downdraft convergence zones in contrast to 40% of non-tornadic mesovortices, 60% of which did not form at all on updraft/downdraft convergence zones. To further the study, more cases and mesovortices should be carefully analyzed to add more validity to the preliminary results found in this study. Forecasters could then utilize findings regarding potential QLCS tornado precursor signatures to provide increased lead time when issuing tornado warnings to the public.

Table 2. Radar signatures associated with tornadic and nontornadic mesovortices. Data quality issues affected the sample size of some signatures.

Signatures	Percentage with Tornadic Mesovortex	Percentage with Nontornadic Mesovortex
Enhanced Area of Spectrum Width	78% (N=18)	60% (N=5)
Rear Inflow Jet Surge	100% (N=18)	100% (N=5)
Z_{DR} Columns	75% (N=12)	50% (N=4)
Enhanced Area of K_{DP} Near Mesovortex	83% (N=12)	50% (N=4)
Long-lived Mesovortex	100% (N=18)	20% (N=5)
Formed on Inbound/Outbound Convergence Zone	83% (N=18)	40% (N=5)

5. ACKNOWLEGEMENTS

I would like to thank Daphne LaDue for all of her help and support during the course of the REU program. I would also like to thank NSF for the opportunity to perform this research and the NWC and OU School of Meteorology for hosting the REU students this summer. Thank you also to my fellow students for their support. Funding was provided by the NSF grant AGS. 1560419.

6. REFERENCES

Atkins, N. T., J. M. Arnott, R. W. Przybylinski, R. A. Wolf, and B. D. Ketcham, 2004: Vortex structure and evolution within bow echoes. Part I: Single-Doppler and damage analysis of the 29 June 1998 derecho. *Mon. Wea. Rev.*, **132**, 2224–2242.

Bluestein, H. B., and M. H. Jain, 1985: Formation of mesoscale lines of precipitation: Severe Squall Lines in Oklahoma during the Spring. *J. Atmos. Sci.*, **42**, 1711–1732.

Chrisman, J. N., 2014: The continuing evolution of dynamic scanning. NEXRAD Now, No. 23, NOAA/NWS/Radar Operations Center, Norman, OK, 8–13. [Available online at http://www.roc.noaa.gov/WSR88D/PublicDocs/NNOW/NNow23a.pdf.]

Crum, T. D., S. D. Smith, J. N. Chrisman, R. E. Saffle, R. W. Hall, and R. J. Vogt, 2013: WSR-88D radar projects – Update 2013. *Proc. 29th Conf. Environmental Information Processing Technologies*, Austin, TX, Amer. Meteor. Soc., 8.1. [Available online at https://ams.confex.com/ams/93Annual/webprogram/Paper221461.html.]

Funk, T. W., K. E. Darmofal, J. D. Kirkpatric, V. L. DeWald, R. W. Przybylinski, G. K. Schmocker, and Y-J. Lin, 1999: Storm reflectivity and mesocyclone evolution associated with the 15 April 1994 squall line over Kentucky and southern Indiana. *Wea. Forecasting*, **14**, 976–993.

Kumjian, M. R., and A. V. Ryzhkov, 2008: Polarimetric signatures in supercell thunderstorms. *J. Appl. Meteor. Climatol.*, **47**, 1940–1961.

Lakshmanan, V., T. Smoth, G. J. Stumpf, and K. Hondl, 2007: The Warning Decision Support System-Integrated Information. *Wea. Forecasting*, **22**, 596–612.

Mahale, V.N., J.A. Brotzge, and H.B. Bluestein, 2012: An Analysis of Vortices Embedded within a Quasi-Linear Convective System Using X-Band Polarimetric Radar. Wea. Forecasting, 27, 1520–1537.

Picca, J. C., M. R. Kumjian, and A. V. Ryzhkov, 2010: Z_{DR} columns as a predictive tool for hail growth and storm evaluation. Preprints, *25th Conf. on Severe Local Storms*, Denver, CO, Amer Meteor. Soc., 11.3. [Available online at https://ams.confex.com/ams/25SLS/webprogram/Paper175750.html.]

Przybylinski, R. W., 1995: The bow echo: Observations, numerical simulations, and severe weather detection methods. *Wea. Forecasting*, **10**, 203–218.

Przybylinski, R. W., G. K. Schmocker, and Y.-J. Lin, 2000: A study of storm and vortex morphology during the intensifying stage of severe wind mesoscale convective systems. Preprints, *20th Conf. on Severe Local Storms,* Orlando, FL, Amer. Meteor. Soc., 173–176.

Snyder, J. C., H. B. Bluestein, G. Zhang, and S. J. Frasier, 2010: Attenuation correction and hydrometeor classification of high-resolution, X-band, dual-polarized mobile radar measurements in severe convective storms. *J. Atmos. Oceanic Technol.*, **27**, 1979–2001.

Trapp, R. J., S. A. Tessendorf, E. S. Godfrey, and H. E. Brooks, 2005: Tornadoes from squall lines and bow echoes. Part I: Climatological distribution. *Wea. Forecasting*, **20**, 23–34.

Wakimoto, R. M., H. V. Murphey, C. A. Davis, and N. T. Atkins, 2006: High winds generated by bow echoes. Part II: The relationship between the mesovortices and damaging straightline winds. *Mon. Wea. Rev.*, **134**, 2813–2829.

Weisman, M. L., and R. J. Trapp, 2003: Low-level mesovortices within squall lines and bow echoes. Part I: Overview and sensitivity to environmental vertical wind shear. *Mon. Wea. Rev.*, **131**, 2779–2803.

Trapp, R.J., and Weisman, M.L., 2003: Low-Level mesovortices within squall lines and bow echoes. Part II: their genesis and implications. *Mon. Weather Rev*. **131**, 2804–2823.